UNIVERSITI
MALAYSIA
PERLIS

Analysis on Sound Absorber Panel Made of Oil Palm Mesocarp Fibre using Delany-Bazley and Johnson-Champoux-Allard Models

Hanif Abdul Latif[1], Izzuddin Zaman[2*], Musli Nizam Yahya[2], Mathan Sambu[3] and Qingshi Meng[4]

[1]*SI Acoustic Sdn Bhd, Jalan Bulan, U5/168 Seksyen U5, Bandar Pinggiran Subang, 40170 Shah Alam, Selangor, Malaysia.*
[2]*Mechanical Failure Prevention and Reliability Research Centre, Faculty of Mechanical and Manufacturing, Engineering, Universiti Tun Hussein Onn Malaysia, 86400 Batu Pahat, Johor, Malaysia.*
[3]*Department of Mechanical Engineering, Faculty of Engineering and Technology, Nilai University, 71800 Nilai, Negeri Sembilan, Malaysia.*
[4]*School of Engineering, Mawson Lakes Campus, South Australia 5095, Australia.*

ABSTRACT

Oil palm mesocarp fibre is seen as one potential of reinforcement in polymers due to its high strength, low cost, environmentally friendly nature and availability. Recently, it has attracted greater interest from academia and industries due to its potential for making a low-cost sound absorption panel. Therefore, this study is obliged to investigate the acoustic characteristics and the physical properties of oil palm mesocarp fibre (OPMF) as a porous material for sound absorbing panel. The measurements of the sound absorption coefficient are determined by using: (1) analytical model of Delany-Bazley, (2) analytical model of Johnson-Champoux-Allard, and (3) experiment of the impedance tube method. A commercial polyurethane (PU) was used as a composite binder during the intermixing process with the fibres. The manufacturing parameters are 10/90, 20/80, 30/70 and 40/60 by wt.% of PU/OPMF. The outcome shows that adding binder compacts the fibre by reducing the pore diameter and porosity, thus increasing the flow resistivity. Results also indicate that Johnson-Champoux-Allard model can justify the overall trend of absorption of the coefficient perfectly in contrast to the Delany-Bazley model. Overall, OPMF with 10 wt.% PU binder displayed greater absorption from low to mid-frequency range and the highest value of noise reduction coefficient of 0.66, while fibres with 20 wt.% PU produced the highest value of sound absorption coefficient of 0.99 at 1000 Hz. The results conclude that oil palm mesocarp displays a potential and brighter prospect to be implemented as a sound absorption panel as demonstrated in this study.

Keywords: Delany-Bazley Model, Johnson-Champoux-Allard Model, Noise Reduction Coefficient, Oil Palm Mesocarp Fibre, Porous Material, Sound Absorption Coefficient.

1. INTRODUCTION

Malaysia at present is one of the largest producers and exporters of palm oil in the world. It is estimated that there is approximately 48.5% of total planted area in hectares in Peninsular Malaysia and about 51.5% in Sabah and Sarawak [1]. Due to the aggressive growth in planting, harvesting and mill operations, the country produces an enormous quantity of oil palm residues such as oil palm frond (OPF), oil palm shell (OPS), oil palm trunk (OPT), oil palm empty fruit bunches (OPEFB) and oil palm mesocarp fibre (OPMF) [2]. Even though these materials are considered wastes, some of them such as OPMF have shown potential as an alternative material for glass and other synthetic fibres. This is coupled with a growing global awareness of environmental, ecological and health issues caused by synthetic materials that drive the use of natural based materials as valuable products.

Corresponding Author: izzuddin@uthm.edu.my

In Malaysia primarily, the Forest Research Institute of Malaysia (FRIM) and the Malaysian Palm Oil Board (MPOB) have conducted fundamental researches to find the potential of using oil palm residues as raw material in diverse engineering applications particularly in automotive components, building materials and the aerospace industry [3–5]. In recent years, there have been an increasing interest in studies on utilizing oil palm mesocarp for producing valuable chemical products by applying a thermochemical conversion process [6,7], hydrothermal pre-treatment [8,9] and combustion of biomass [10]. However, to the best knowledge of authors, the study related to OPMF's sound performance or sound absorption behaviour has yet to be performed.

These days, noise has turned out to be one of the many factors that influence human health and environment due to the advancement of modern industry and traffic systems. Hence, the need for effective techniques for reducing noise has become a major issue, and the latest is using waste material and natural fibres as sound absorber. This is because the use of these materials not only have potential to reduce noise, but are also able to solve environmental pollution problems. For example, several researchers have succeeded in developing agricultural waste to produce sound absorption panels. Yang *et al.* [11] studied the possibility of using rice straws and waste tires as sound insulation boards and they found that the acoustical insulation of composite panel was superior to other wood-based panel products. Meanwhile, Berardi and Iannace [12] examined the acoustical characterization of several natural fibres such as kenaf, wood, hemp, coconut, cork, cane, cardboard, and sheep wool.

Some of the researchers also mixed the raw material with an adequate binder or adhesive to create a solid sample of the sound absorber, even though this is not considered a new method in the polymer composite. For instance, Nor *et al.* [13] reported that by applying the binder it could improve the acoustic properties especially in the high-frequency range. Maderuelo-Sanz *et al.* [14] demonstrated that the sample porosity decreases when the percentage of polyurethane (PU) binder increases, thus enhancing the acoustic flow resistivity. Furthermore, Borlea *et al.* [15] mixed the pine sawdust with commercial PU binder with two different weight percentages 20% and 30% and found that the sample with 30 wt.% improves acoustic properties better than the 20 wt.% of PU binder in a low-frequency range. However, 20 wt.% shows the highest sound absorption coefficient of 0.9 at a high-frequency range between 3150 – 6300 Hz.

In spite of these studies, there is still little knowledge about sound absorption behaviour of waste materials, in particular to OPMF. Therefore, this study is devoted to investigating the potential use of OPMF in acoustic absorption application. The effect of binder in determining the optimum acoustic performance (e.g. sound absorption coefficient and noise reduction coefficient) was analysed in this research, including the physical properties measurement such as flow resistivity, tortuosity, porosity, and characteristic length. In order to better understand the sound absorption properties of OPMF, the experimental results were validated with the analytical prediction models of Delany-Bazley and Johnson-Champoux-Allard.

2. MATERIAL SELECTION AND PREPARATION

2.1 Raw Material

Oil palm mesocarp fibres were provided by Oil Palm Processing Sdn. Bhd., Kluang, Johor, Malaysia. The raw fibre consists of a mixture of the outer skin (exocarp), shell (endocarp), crushed kernel and mesocarp. Prior to sample preparation, the mesocarp fibres underwent several pre-treatment processes to remove unwanted dirt and materials such as kernels and endocarp. This includes the soaking of fibres in clean water for one week before being dried naturally under the sun and then heated in the oven at 70 ºC for 4 hours in order to remove

residual water. The cleaned fibres were finally cut using a crusher machine into 10–15 mm lengths as shown in Figure 1. The fibers were then milled by the rotor mill machine to get fine sizes of random fibers before they were sieved using a sieve shaker machine with a ring size of 200 μm to obtain a uniform size of the filler. Meanwhile, polyol and isocyanate were purchased from Dwicira Resources Sdn. Bhd. in order to form polyurethane (PU) binders.

Figure 1. Oil palm Mesocarp fibre 10-15 mm in length.

2.2   Sample Preparation

There were four weight percentages of PU binders prepared with OPMF in this research, which range from 10 to 40 wt.%. At a ratio of 0.5 of isocyanate to polyol the PU binders dropped into arrays of OPMF, followed by stirring for 10 minutes to achieve homogeneous dispersion. The mixture was then transferred into the cylindrical moulds of 28 mm and 100 mm diameters with a thickness of 50 mm, and later curing at room temperature for 24 hours. The large diameter of OPMF/PU sample is for the low-frequency test and the small diameter sample is for the high-frequency test.

3.   METHODS

3.1   Experimental Measurement using Impedance Tube

There are two parameters measured in this research to investigate the acoustical properties of porous absorbent: the sound absorption coefficient and the noise reduction coefficient (NRC). The impedance tube method was implemented to investigate these acoustical properties. The impedance tube comprises two different tubes of 28 mm and 100 mm diameters, two ¼-inch pressure microphones type GRAS-40BP, preamplifier, and two channels of data acquisition system 01dB which was connected to the software SCS8100. This tube configuration represents the basis, standard system setup for sound absorption coefficient and impedance measurements. The microphones location is established based on the standard method, by calculating the transfer function of two fixed microphones which are located at two different positions in the tube wall. The calibrator used for microphone sensitivity was Larson Davis CAL 200. The test was performed according to ISO 10534-2, where the measurement of the sound absorption properties of the material is based on the two microphones transfer-function method. The set up for the impedance tube measurement system used in the laboratory work is illustrated in Figure 2.
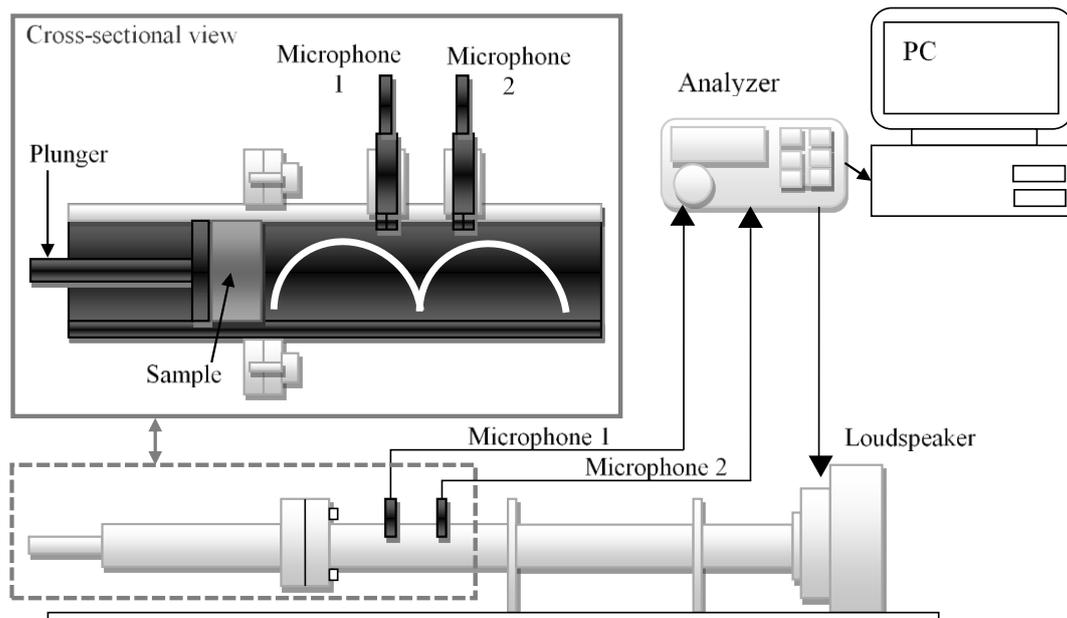
Figure 2. Schematic sketch of impedance tube setup.

Noise reduction coefficient, on the other hand is a single number rating system for indexing the ability of materials to absorb sound. It is measured based on the average value of sound absorption coefficient over human speech frequencies that range at 250, 500, 1000, and 2000 Hz [16]. The NRC can be calculated using Equation (1), where α is the sound absorption coefficient.

$$NRC = \frac{\alpha_{250Hz} + \alpha_{500Hz} + \alpha_{1000Hz} + \alpha_{2000Hz}}{4} \tag{1}$$

3.2   Delany-Bazley Model

In this section, an empirical formula based on Delany-Bazley model (DBM) is utilized for the estimation of characteristic impedance and propagation coefficient of oil palm mesocarp fibres. The model is considered very simple and an easy approximation to the solution as it uses only frequency and flow resistivity parameters which are an intrinsic property of the material [17,18].

The characteristic of impedance Z_c can be obtained by:

$$Z_c = \rho_0 c_0 F_1(X) \tag{2}$$

And the wavenumber, k by:

$$k = \frac{2\pi f}{c_0} F_2(X) \tag{3}$$

Where ρ_0 is the density of air, c_0 and f are speed and frequency of sound. While, $F_1(X)$, $F_2(X)$ and X are given in Equations (4)–(6), respectively:

$$F_1(X) = 1 + 0.0571X^{-0.754} - j0.087X^{-0.732} \tag{4}$$

$$F_2(X) = 1 + 0.0978X^{-0.700} - j0.189X^{-0.595} \tag{5}$$

$$X = \frac{\rho_0 f}{\sigma} \tag{6}$$

Where σ the flow resistivity of the fibrous material and j is an imaginary number. This model is only applicable when the boundary of X falls in the range of $0.01 < X < 1.0$, and the flow resistivity measurement in the range of $1000 \leq \sigma \leq 50000 \ Nsm^{-4}$. Thus, the frequency is dependent on the sound speed, c_{eq} and density of a highly porous material, ρ_{eq} according to this model can be expressed as follows:

$$c_{eq} = \frac{\omega}{k} = \frac{c_0}{F_1(X)} \tag{7}$$

$$\rho_{eq} = \frac{Z_c}{C_{eq}} = \frac{Z_c k}{w} = \rho_0 F_1(X) F_2(X) \tag{8}$$

As mentioned earlier this approach only depends on the frequency and flow resistivity to study the behaviour of porous materials, so it cannot be expected to provide perfect predictions [19].

3.3 Johnson-Champoux-Allard model

This model is devoted to the semi-phenomenological theoretical model of porous absorbents. Several researchers have been engaged in the generating of the model where models of Allard and Atalla [19], Champoux and Allard [20] and Johnson *et al.* [21] were combined to produce a simple phenomenological model. There are two parameters required in this model which are the effective density, ρ_e and the effective bulk modulus of air in the material, K_e. Both can be expressed in the following Equations (9) and (10), respectively:

$$\rho_e = k_s \rho_0 \left[1 + \frac{\sigma\varepsilon}{j\omega\rho_0 k_s} \sqrt{1 + \frac{4jk_s^2 \eta\rho_0\omega}{\sigma^2 \Lambda^2 \varepsilon^2}} \right] \tag{9}$$

$$K_e = \frac{\gamma P_0}{\gamma - (\gamma - 1) \Big/ \left(1 + \frac{8\eta}{j\Lambda'^2 N_p \omega\rho_0} \sqrt{1 + \frac{j\rho_0 \omega N_p \Lambda'^2}{16\eta}} \right)} \tag{10}$$

Where k_s, ε, Λ and Λ' are the tortuosity, porosity, viscosity and thermal characteristic length of porous material, respectively; ω is angular frequency, η is the viscosity of air, γ is the ratio of specific heat capacity for air (≈ 1.4) and P_0 is atmospheric pressure. The Prandtl number, N_p can be calculated from Equations (11)–(13):

$$N_p = \left(\frac{\delta_v}{\delta_h} \right)^2 \tag{11}$$

$$\delta_v = \sqrt{\frac{2\eta}{\rho\omega}} \tag{12}$$

$$\delta_h = \sqrt{\frac{2\eta\kappa}{\rho c_p \omega}} \tag{13}$$

Where δ_v and δ_h is the thickness size of the viscous and thermal boundary layer, respectively; κ is the thermal conductivity of air and c_p is the specific heat capacity of air at constant pressure. In this study, the fibre structure is assumed as elastic cylindrical fibres and the layer of porous material with identical parallel pores is considered perpendicular to the surface (normal incidence). After determining the Equations (9) and (10), the characteristic impedance, Z_c and the complex wave number, k in a pore can be determined by:

$$Z_c = (K_e \rho_e)^{1/2} \tag{14}$$

$$k = \omega \left(\frac{\rho_e}{K_e}\right)^{1/2} \tag{15}$$

3.4 Flow Resistivity Measurement

The flow resistivity of the samples is measured using the formulation that was developed by Ballagh [22]. Based on the derived formulation, there is a close relationship between flow resistivity, density, and fibre diameter. For this study, Equation (16) is implemented to determine the flow resistivity, σ.

$$\sigma = 490 \frac{\rho_{bulk}^{1.61}}{d_{fibre}} \tag{16}$$

Where d_{fiber} is diameter fibre and ρ_{bulk} is the bulk density. Each fibre is assumed to be a perfect cylindrical shape. Here, the fibres were taken randomly, and the diameter fibres were measured by using a digital microscope scan. On the other hand, the bulk density was measured experimentally via porosity measurement.

3.5 Porosity Measurement

The porosity, ε of each sample can be determined by using Equation (17) by measuring two variables which are pore volume, V_p and bulk volume, V_b.

$$\varepsilon = \frac{V_p}{V_b} \tag{17}$$

$$V_p = \frac{(W_s - W_d)}{\rho_s} \tag{18}$$

$$V_b = \frac{W_s - W_i}{\rho_s} \tag{19}$$

Where W_s is the weight of the saturated sample, W_d is the weight of the dried sample, W_i is the weight of the immersed sample and ρ_s is the density of the saturated liquid. In this experiment, the weight of the dried sample is measured in a vacuum condition in order to produce a more accurate result [23].

3.6   Tortuosity Measurement

Tortuosity is linked to the inertial part of the force between fluid and frame. There are various methods to get the tortuosity accurately but in order to avoid samples getting damaged from the soaking process, the tortuosity, k_s is measured by using Equation (20) according to Umnova *et al.* [24].

$$k_s = \frac{1}{\sqrt{\varepsilon}} \qquad (20)$$

3.7   Characteristic Lengths Measurement

In this study, the viscous characteristic length can be found using the empirical equation defined by Allard and Atalla [19]. The fibres are assumed to lie in planes parallel to the surface of the layers and the macroscopic air velocity is perpendicular to the direction of the fibres at normal incidence. The fibres are also assumed as an infinitely long cylinder having a circular cross-section with a known radius. The viscosity characteristic length, Λ is given by:

$$\Lambda = \frac{1}{2\pi r l} \qquad (21)$$

Where r and l are the radius and total length of the fibre, respectively. The total length of fibre can be calculated from the following equation:

$$l = \frac{1}{\pi r^2 \left(\dfrac{\rho_{bulk}}{\rho_{fibre}}\right)} \qquad (22)$$

Where ρ_{fibre} is the density of the fibre. The thermal characteristic length was evaluated from Equation (23).

$$\Lambda' = 2\Lambda \qquad (23)$$

4.   RESULT AND DISCUSSION

4.1   Physical Properties within Porous Absorbents

Average values of the physical properties of the OPMF samples are tabulated in Table 1. Obviously, it can be seen that different percentage of PU and OPMF contents produces variation in their physical properties. Large differences observed in flow resistivity, demonstrate the significant effect of the PU binder on the bulk density and diameter of produced fibres [22,25]. The range of flow of resistivity, calculated using the Ballagh formula for the porous material is obtained from 15,000 to 37,000 Nms^{-4} as shown in Table 1. With the exception of the pure OPMF sample, the flow resistivity gradually increases with the increase of the PU binder concentration for the combined mixture with OPMF particle size ranging from 200 microns to 1 mm [26]. Meanwhile, as expected the porosity of OPMF with 40 wt.% PU binder shows the lowest value followed by 30 wt.%, 20 wt.% and 10 wt.% PU binder. This is because the binder compacts the fibre tightly causing less of a hollow space within the fibre composite [27]. Figure 3 illustrates the relationship between the porosity and flow resistivity where reducing the porosity results in an increased flow of resistivity.

Table 1 Effect of PU binder on physical properties of OPMF

Sample OPMF with PU loading (wt.%)	Flow Resistivity (Nms^{-4})	Porosity	Tortuosity	Viscous characteristic length (μm)	Thermal characteristic length (μm)
0	37,415.52	0.847	1.087	97.81	195.62
10	17,201.09	0.882	1.065	582.37	1164.74
20	17,566.14	0.801	1.117	613.73	1227.46
30	18,594.63	0.766	1.143	629.27	1258.54
40	21,439.48	0.639	1.251	700.15	1400.3
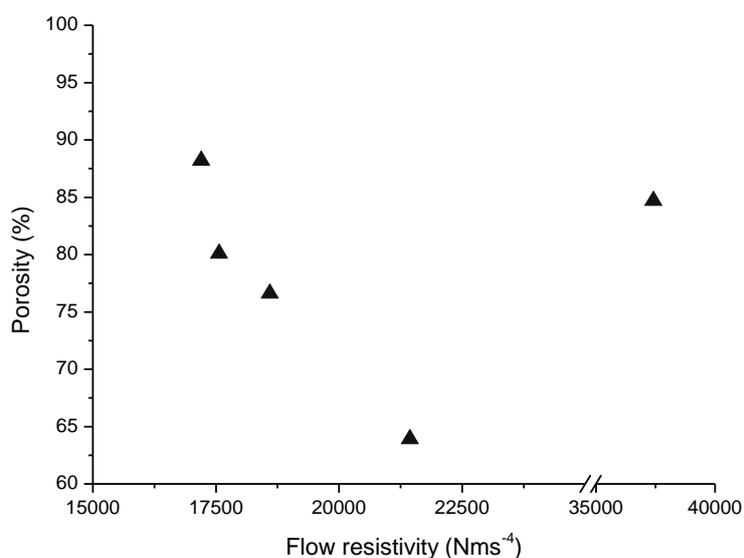
Figure 3. The porosity as a function of the flow resistivity for OPMF samples.

On the other hand, the PU binder is also found to be influencing the average path length of a pore and thereby giving a higher tortuosity. This is due to the random arrangement of fibres creating more tortuosity but reducing pores that may affect the acoustical performance [28]. The range of the tortuosity is from 1.087 to 1.251. In similar cases, the characteristic lengths were found to have increased for both viscous and thermal, by increasing the loading percentage of binder. These outcomes indicate that the binder affects the radius of the pores and the stiffness of the material.

4.2 Acoustical Properties

Figure 4 shows that the sound absorption coefficient against the frequency spectra for OPMF samples with different percentages of PU binder is measured by impedance tube. It was found that the absorption coefficients for most of OPMF samples initially increased from 0.1 to ~0.9 but then decreased to ~0.7 between 1000 Hz to 3000 Hz before reaching maximum peak of ~1 at 4000 Hz. Basically, the sound absorption spectra obtained are in good agreement with the previously published data where it shows a standard pattern for porous absorbent materials [16,29]. The result indicated that all OPMF samples demonstrated a higher sound absorption coefficient at the medium to high-frequency range with the average absorption of above 0.7.
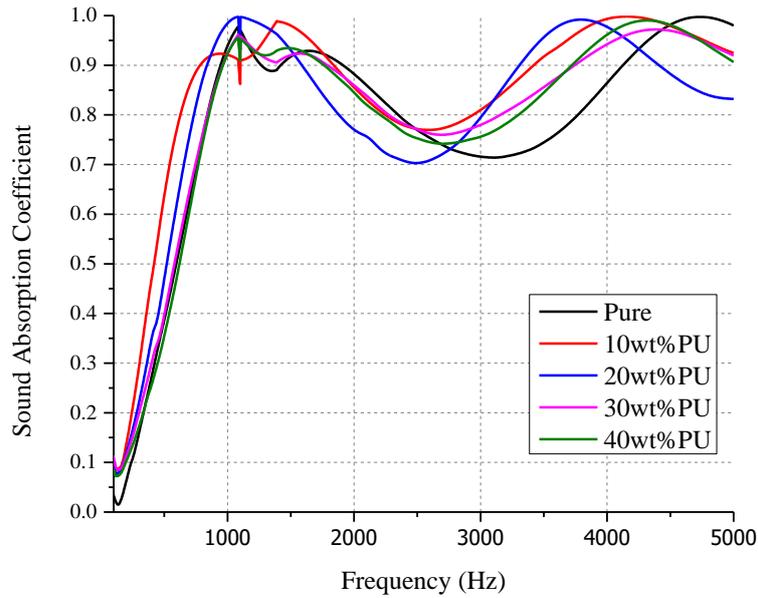
Figure 4. Variation of sound absorption coefficient of OPMF at different PU concentration.

The best acoustic performance over the frequency range of interest is obtained for the sample OPMF with 10 wt.% PU binder. For this sample, the maximum value of the sound absorption coefficient is 0.96 and 0.98, respectively achieved at the frequency of 1400 Hz and 4100 Hz. This is attributable to the high porosity obtained by the sample of 0.882. However, the sample with 20 wt.% PU binder displays the highest value of sound absorption of 0.99 at 1000 Hz. This result demonstrates that the OPMF sample with low concentration PU binder which in this case is below 20 wt.% can improve sound absorption at the medium frequency range, thus indicating that the cavity resonances were suppressed by the damping of fibre causing loss of sound energy via friction with the pore walls [28]. In addition, the PU binder also contributes to the improvement in the low to medium frequencies because of the membrane effect that produces greater depth to the resonant structures and the interconnected pores of the sample prevent the energy [30].

By contrast, there was no improvement at the low-medium frequencies for OPMF samples with 30 wt.% and 40 wt.% PU binder. Nevertheless, both samples were found to improve the absorption coefficient in the frequency range of 2500 Hz to 4500 Hz compared to pure OPMF without any binder. The acoustic performance of the OPMF with 30 wt.% PU is similar to the 40 wt.% PU, showing the maximum absorption coefficient at frequency 4150 Hz. The mechanism involved in sound absorption for these samples are still the same where the sound waves are dissipated through interaction (mechanical friction) that occurred at the boundaries between PU binder and fibre. Although these samples are not favourable in terms of sound absorption performance compared to the other two preceding samples, the mechanical properties are slightly improved due to many pores being filled with a binder [11].

Table 2 tabulates the values of the sound absorption for OPMF samples in the octave bands frequency (250 Hz, 500 Hz, 1000 Hz and 2000 Hz), together with the noise reduction coefficient (NRC). It was found that NRCs for all samples are above 0.5, thus indicating that OPMF is highly absorptive [31]. Of these samples, OPMF with 10 wt.% PU binder demonstrates the optimum value with the most significant increase of NRC at 0.66. As the binder content increases, the NRC of OPMF samples significantly dropped. The NRC reduction is explained by the fact that adding more percentages of PU binder affect the physical properties and consequently give impact on the sound absorption.

Table 2 Effect of PU binder on noise reduction coefficient of OPMF

Sample OPMF with PU loading (wt.%)	Frequency (Hz)				NRC
	250	500	1000	2000	
0	0.11	0.39	0.94	0.88	0.58
10	0.21	0.64	0.92	0.86	0.66
20	0.17	0.47	0.98	0.77	0.60
30	0.15	0.40	0.92	0.86	0.58
40	0.13	0.35	0.92	0.85	0.56

Table 3 compares the NRC values of the optimum OPMF sample obtained from this study with the other type of natural fibres as well as synthetic fibres from previous research studies. OPMF with 10 wt.% PU binder improves NRC far more effectively than other natural fibers such as corn, coir, grass, sugarcane and bamboo fibre. The sample, however, was found to be slightly 0.10 lower than the synthetic glass wool fibre. Nevertheless, this comparison indicates that the oil palm Mesocarp fiber with 10 wt.% binder is capable to be a good sound absorption panel when looking at the environmental, ecological and health effects of synthetic fibre.

Table 3 Noise reduction coefficient of OPMF and other type of fibres from previous research

Material	NRC	References
10wt.% PU/OPMF	0.66	-
Corn fibre	0.33	Fouladi et. al [32]
Coir fibre	0.40	Fouladi et. al [32]
Grass fibre	0.41	Fouladi et. al [32]
Sugarcane fibre	0.42	Fouladi et. al [32]
Bamboo	0.53	Koizumi et. Al [34]
Polyurethane	0.58	Bies and Hansen [35]
Glass wool	0.76	Bies and Hansen [35]

4.3 Analytical Modelling

For sufficient acoustic material to be used as a porous absorber, it is desirable to predict acoustical absorption in function of frequency. These days, there are many models available to predict the porous absorbent acoustic features which can save time and numerous trial experiments. In this research, the Delaney-Bazley model and Johnson-Champoux-Allard model were employed to model the acoustic properties of the OPMF samples as per described in Sections 3.2 and 3.3, respectively. Figures 5–9 show the comparison between the analytical models and the measured absorption coefficient for samples OPMF used in this work. The predicted results of the Delaney-Bazley model and Johnson-Champoux-Allard model follow closely the experimental results throughout the considered frequency range.
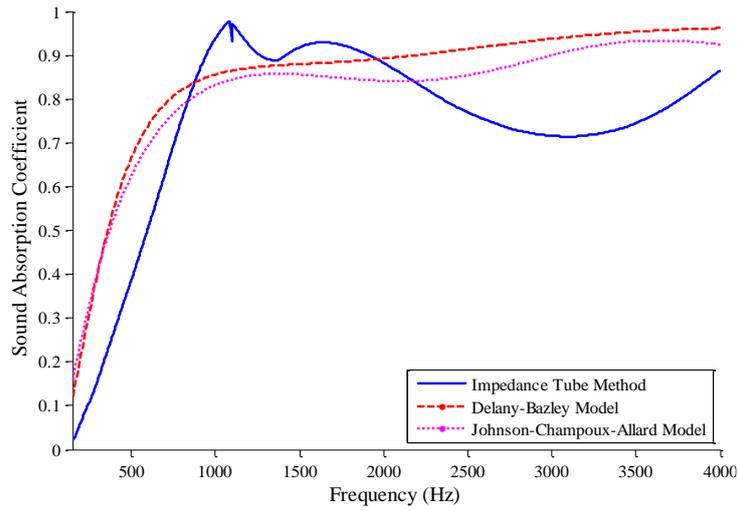
Figure 5. Comparison between the experimental results and prediction models for pure OPMF.
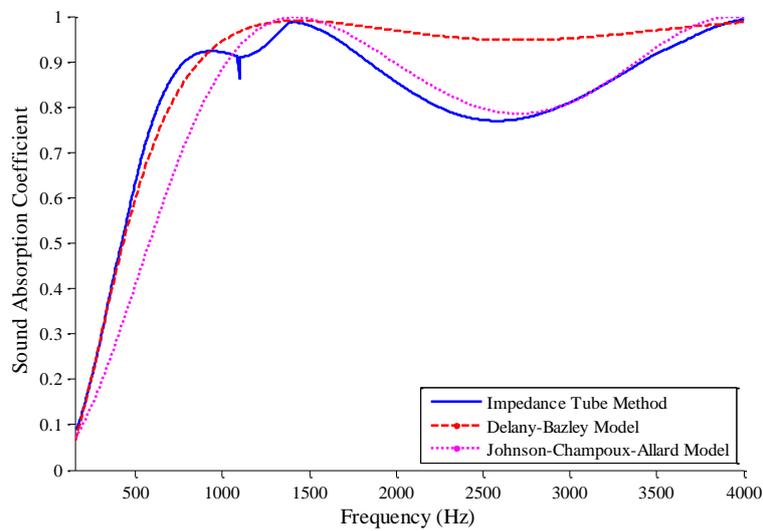
Figure 6. Comparison between the experimental results and prediction model for OPMF sample with 10 wt.% PU binder.
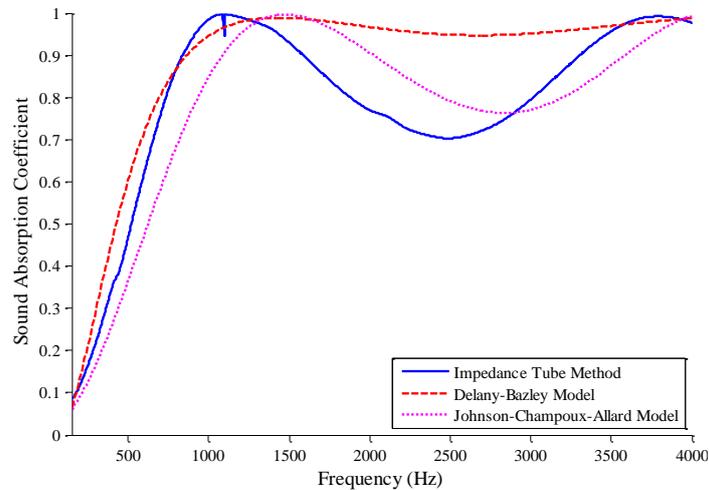
Figure 7. Comparison between the experimental results and prediction models for OPMF sample with with 20 wt.% PU binder.
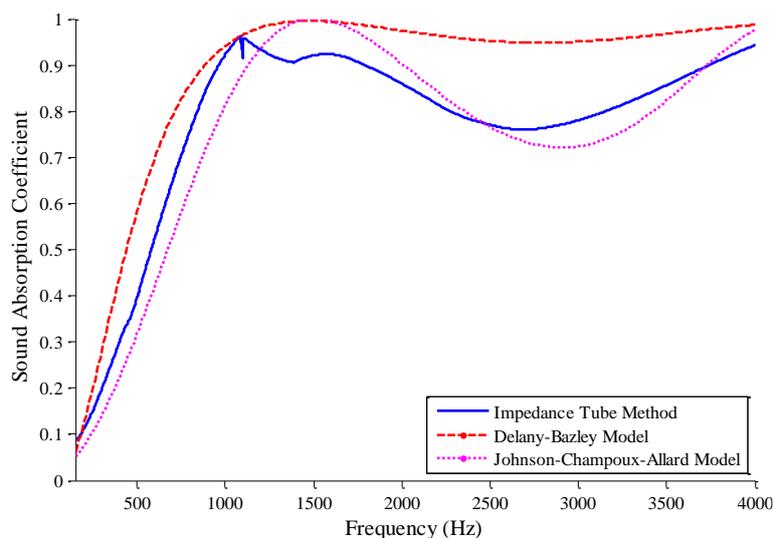
Figure 8. Comparison between the experimental results and prediction models for OPMF sample with with 30 wt.% PU binder.
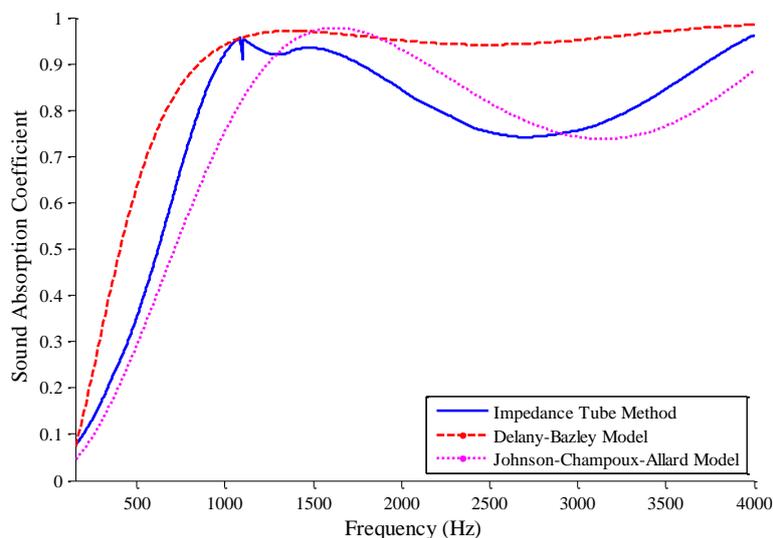
Figure 9. Comparison between the experimental results and prediction models for OPMF sample with 40 wt.% PU binder.

From Figures 5–9, it can be seen that except for pure OPMF, the Delaney-Bazley model predicts the sound absorption of OPMF samples with PU binder well particularly in the frequency range of less than 1500 Hz. However, the error becomes larger towards the medium to high-frequency range. The discrepancies of the prediction might be because the model is developed by a simple empirical approach and fast approximation using one parameter which is the flow resistivity [32]. Despite this disadvantage, the Delaney-Bazley model has shown better predictions in the classical fibrous material where the porosity is close to 1, for example, glass wool [30]. The glass wool normally has open pores where the connection from one pore to another pore is strong. According to Oliva and Hongisto [33], the Delaney-Bazley model is suitable for the low-frequency range and capable to give good results between 4000 Hz to 10000 Hz.

Meanwhile, the Johnson-Champoux-Allard model produces better sound absorption predictions compared to the previous model where it displays a similar pattern of spectra and match the acoustic behaviour of OPMF samples. It showed that the model was in line with the

experimental results, thus proving the Johnson-Champoux-Allard model could be used successfully as an analytical tool for porous material such as OPMF. However, as the frequency and PU binder concentration increases, the position of the second peak could not be properly estimated. Anomalies in the results may be because the model does not take into account the binder that was used in the sample separately. In this case, the binder is assumed as part of the fibres that covered their surfaces and filled the pore between them [32].

5. CONCLUSION

This work shows an investigation of oil palm mesocarp fibre and its acoustical performance. The influences of binder addition on the physical properties and the sound absorption coefficient of oil palm mesocarp were determined. In the study, the experiment was conducted by adopting an impedance tube method, while two analytical approaches were implemented to support the analyses, namely the Delaney-Bazley model and the Johnson-Champoux-Allard model. The experimental result show that the OPMF sample with 10 wt.% of PU binder demonstrated the best acoustic performance in terms of noise reduction and sound absorption coefficients in most of the medium to high frequencies, although 20 wt.% PU binder displayed the highest sound absorption coefficient of 0.99 at 1000 Hz. Moreover, by increasing binder concentration shifted the maximum and minimum peaks toward a low frequency. In terms of the prediction model, the Johnson-Champoux-Allard model had the advantage over Delaney-Bazley's analytical model where it not only displayed a similar pattern of sound absorption but also predicted the resonance peaks very well. The outcome of this research clearly shows the potential of oil palm mesocarp fibre as a promising material to be utilized as a sound absorber panel that can replace the use of synthetic materials. The work also can be served as a guide for future designing of effective porous absorbers.

REFERENCES

[1]   Malaysian oil palm statistics 2017 - 37th edition, Economics and Industry Development Division, MPOB, Malaysian Palm Oil Board, (2018).
[2]   Singh P., Sulaiman O., Hashim R., Peng L. C., Singh R. P., Environment, Development and Sustainability **15**, 2 (2013) 367-383.
[3]   Shaari N. Z. K., Lye O. T., Ahmad S., Journal of Oil Palm Research **18** (2006) 198-203.
[4]   Kushairi A., Singh R., Ong-Abdullah M., Journal of Oil Palm Research **29** (2017) 431-439.
[5]   Sari N. H., Rahman A., Syafri E., International Journal of Nanoelectronics and Materials **12**, 2 (2019) 193-204.
[6]   Luangkiattikhun P., Tangsathitkulchai C., Tangsathitkulchai M., Bioresource Technology **99**, 5 (2008) 986-997.
[7]   Awalludin M. F., Sulaiman O., Hashim R., Nadhari W. N. A. W., Renewable and Sustainable Energy Reviews **50** (2015) 1469-1484.

[8]   Jansar K. N., Roslan A. M., Hassan M. A., Pertanika Journal of Scholarly Research Reviews **4**, 1 (2018) 31-40.

[9]   Zakaria M. R., Norrrahim M. N. F., Hirata S., Hassan M. A., Bioresource Technology **181** (2015) 263-269.

[10]   Idris S. S., Rahman N. A., Ismail K., Bioresource Technology **123** (2012) 581-591.

[11]   Yang H. S., Kim D. J., Lee Y. K., Kim H. J., Jeon J. Y., Kang C. W., Bioresource Technology **95**, 1 (2004) 61-65.

[12]   Berardi U., Iannace G., Building and Environment **94** (2015) 840-852.

[13]   Nor M. J. M., Ayub M., Zulkifli R., Amin N., Fouladi M. H., Journal of Applied Sciences **10**, 22 (2010) 2887-2892.

[14]   Maderuelo-Sanz R., Barrigon Morillas J. M., Martín-Castizo M., Gomez Escobar V., Rey Gozalo G., Latin American Journal of Solids and Structures **10**, 3 (2013). 585-600.

[15]   Borlea A., Rusu T., Ionescu S., Cretu M., Ionescu A., Romanian Journal of Acoustics and Vibration **8**, 2 (2011) 95-98.

[16]   Sambu M., Yahya M. N., Latif H. A., Zaman I., Ghazali M. I., International Review of Mechanical Engineering **10**, 4 (2016) 284-288.

[17]   Delany M. E., Bazley E. N., Applied Acoustics **3**, 2 (1970) 105-116.

[18]   Dunn I. P., Davern W. A., Applied Acoustics **19**, 5 (1986) 321-334.

[19]   Allard J., Atalla N., Propagation of sound in porous media: Modelling sound absorbing materials. United Kingdom: John Wiley & Sons, (2009).

[20]   Champoux Y., Allard J. F., Journal of applied physics **70**, 4 (1991) 1975-1979.

[21]   Johnson D. L., Koplik J., Dashen R., Journal of fluid mechanics **176** (1987) 379-402.

[22]   Ballagh K. O., Applied Acoustics **48**, 2 (1996) 101-120.

[23]   Panneton R., Gros E., ACTA Acustica united with Acustica **91**, 2 (2005) 342-348.

[24]   Umnova O., Attenborough K., Shin H. C., Cummings A., Applied Acoustics **66**, 6 (2005) 607-624.

[25]   Kino N., Ueno T., Applied Acoustics **69**, 7 (2008) 575-582.

[26]   Luu H. T., Perrot C., Panneton R., ACTA Acustica united with Acustica **103**, 6 (2017) 1050-1063.

[27]   Kim K.-Y., Doh S. J., Im J. N., Jeong W. Y., An H. J., Lim D. Y., Fibers and Polymers **14**, 4 (2013) 639-646.

[28]   Latif H. A., Yahya M. N., Zaman I., Sambu M., Ghazali M. I., Hatta M. N. M., ARPN Journal of Engineering and Applied Sciences **11**, 4 (2016) 2462-2466.

[29]   Wang C. N., Torng J. H., Applied Acoustics **62**, 4 (2001) 447-459.

[30]   Garai M., Pompoli F., Applied Acoustics **66**, 12 (2005) 1383-1398.

[31]   Lee J., Kim G. H., Ha C. S., Journal of applied polymer science **123**, 4 (2012) 2384-2390.

[32]   Fouladi M. H., Ayub M., Nor M. J. M., Applied Acoustics **72**, 1 (2011) 35-42.

[33]   Oliva D., Hongisto V., Applied Acoustics **74**, 12 (2013) 1473-1479.

[34]   Koizumi T., Tsujiuchi N., Adachi A., In: High Performance Structures and Composites **59**, (2002) 157-166.

[35]   Bies D., Hansen C., Engineering Noise Control: Theory and Practice. New York, NY, USA: Taylor and Francis, (2009).